Resilience Indices for Power/Cyberphysical Systems

Soumyabrata Talukder, *Graduate Student Member, IEEE*, Mariam Ibrahim, *Member, IEEE*, and Ratnesh Kumar, *Fellow, IEEE*

***Abstract*—An engineered system is designed to deliver certain *performance* related to its quality-of-service, and while doing so, it must also maintain *stable* operation. Resilience of a system is its ability to continue to offer system performance stably, while withstanding any adverse events. Motivated by this concept, we propose to measure the resilience level of a power system by quantifying its *stability level* as measured by: transient stability margin (TSM), critical clearance time (CCT), relay margin (RM), and load security margin (LSM), as well as its *performance level* as measured by: load loss (LL) and recovery/repair time (RT) while being exposed to adverse events. For comparability, we also propose a normalization for each of the 6 measures to a number in the unit interval [0, 1], which is scale-invariant, and further probabilistically average each of those across all possible sequences of faults (of a specified length) against their occurrence probabilities to arrive at a set of 6 unit-interval valued indices. New polynomial complexity algorithms (in the number of generators) are proposed for estimating TSM (in form of volume of region of stability) and CCT; new quadratic program formulation for precise computation of RM is developed and implemented; also, new security and stability informed notions of LSM and LL are introduced and implemented by extending continuation power flow. Such quantification of resilience levels provides a numerical measure to compare the relative abilities of different power grids to withstand the impact of sequences of adverse events. The proposed approach is illustrated by computing and comparing the resilience of three similar power system topologies differing only in the location of generators. The framework is further validated by implementing it on the IEEE 30-bus test system.**

***Index Terms*—Contingency screening, critical clearance time (CCT), cyberphysical systems (CPSs), region of stability (RoS), relay margin (RM), resiliency, stability margin, static security margin.**

I. Introduction

RESILIENCE is a key system property of its ability to continue to provide quality-of-service/*performance* withstanding disruptive faults/attacks [1], which in turn requires its continued *stable* operation. Given the frequency of recent outages [2] in power systems, a class of critical infrastructures, understanding and quantifying its resilience are of paramount importance. Since the occurrence of disturbances and faults can affect both the *stability* and the *performance* levels, one way to quantify the resilience level is by quantifying the post-fault-clearance stability level as well as performance level. In our work, the *stability levels* are measured using: transient stability margin (TSM), critical clearance time (CCT), relay margin (RM), and load security margin (LSM), while the *performance levels* are measured using: load loss (LL) and recovery time (RT).

Resilience is more encompassing than *security*, which for a power system, refers to its ability to survive imminent (high probability) disturbances and contingencies without any consequential interruption of customer service [3], as mandated by the North American Electric Reliability Council (NERC) [4]. However, the levels of security/stability/relay margins and clearance/recovery times may differ, which can impact the effect of exposure to newer contingencies. Thus, a measure of resilience of a power system against disruptive contingencies should also include their impacts beyond the interruption to customer service, namely, impacts on security/stability/relay margins and the clearance/recovery times, as it has been done in our proposed approach. According to the National Infrastructure Advisory Council (NIAC) [5], the resilience of an infrastructure is defined to be its ability to reduce the magnitude and/or duration of disruptive events. Rather than providing a specific way of quantifying resilience, NIAC report [5] maps resilience to: *robustness, resourcefulness, rapid recovery*, and *adaptability*. In our setting, the notions of TSM, CCT, RM, LSM, LL reflect both the initial *robustness* of the system as well as its dynamic *resourcefulness* (i.e., reconfiguration or recovery upon faults), whereas the notion of RT captures *rapid recovery*. Finally, the *adaptation* is enabled by evaluation of the proposed 6 measures and identifying any need for system enhancements to improve those measures.

Prior related works of the other researchers is summarized in Section I-A, while this paragraph discusses our own initial work on the topic [6], in which only the quantification of TSM in terms of size of region of stability (RoS), the amount of load service, and RT was proposed. The RoS was estimated by a backward reach computation, starting from an equilibrium point and following the gradient of the potential energy function by solving a Hamilton–Jacobi–Isaacs PDE using the level set toolbox [7], having computational complexity *exponential* in the number of generators.

Manuscript received September 25, 2019; revised May 1, 2020 and July 7, 2020; accepted August 10, 2020. Date of publication September 16, 2020; date of current version March 17, 2021. This work was supported in part by the National Science Foundation under Grant CCF-1331390, Grant ECCS-1509420, Grant PFI-1602089, and Grant CSSI-2004766. This article was recommended by Associate Editor D. Yue. *(Corresponding author: Soumyabrata Talukder.)*

Soumyabrata Talukder and Ratnesh Kumar are with the Department of Electrical and Computer Engineering, Iowa State University, Ames, IA 50010 USA (e-mail: talukder@iastate.edu; rkumar@iastate.edu).

Mariam Ibrahim is with the Department of Mechatronics Engineering, German Jordanian University, Amman 11180, Jordan (e-mail: mariam.wajdi@gju.edu.jo).

Color versions of one or more of the figures in this article are available online at https://ieeexplore.ieee.org.

Digital Object Identifier 10.1109/TSMC.2020.3018706

The analysis was further limited to a single fault/attack sequence.

The contributions of this article are summarized as follows.

1) A key contribution of this article is to introduce stability as well as performance-based measures to characterize the resilience level of a power system in terms of six indices: TSM, CCT, RM, LSM, LL, and RT values of the subsystems resulting from different possible fault-sequences (the approach of analyzing such subsystems is inspired from [8]). Next, these values are normalized to make them uniform in the range [0, 1] and thus comparable. Finally, those are averaged against the occurrence probabilities of the fault-sequences to provide a set of 6 unit-interval valued indices for each power system. It substantially extends the concepts and methods proposed in our earlier work [6]. Also, the proposed 6 indices are quite comprehensive, and in fact, only to 2 of those (LL and RT) are needed to derive a recently proposed measure, namely, time-integral of load served (TILS) [9], [10]. The other indices offered by our proposed framework reveal additional insights related to resilience.
2) We present a novel polynomial complexity computation (in the number of generators) of TSM, as measured by the volume of RoS. We do this by extending a sum of squares (SoS) optimization-based method, which was introduced in [11], and thereafter, has been employed to solve numerous control and stability related problems (see for example [12]). We propose a SoS-based method to find a Lyapunov function, and its sublevel set estimates the RoS [13], [14]. Our estimate of the size of RoS is in the form of a maximal volume inscribed ellipsoid, obtained employing a linear matrix inequality (LMI)-based optimization, adopting the method of finding the maximum volume ellipsoid inscribed in an intersection of ellipsoids [15]. This resulting approach is of polynomial complexity (in the number of generators). The earlier approaches (e.g., [13]) used numerical integration to compute the volume of RoS, which is of exponential complexity. Also, the backward reachability-based method adopted in [6] for approximating RoS scales exponentially with respect to the number of generators, and it further requires a well-defined energy function [16], which does not exist in general for a power system possessing transfer conductance (see [17], [18]). Our approach works for power systems with transfer conductance, and also for those possessing larger relative angles at the equilibrium, in contrast to several other approaches for estimating RoS [6], [14], [19]–[23].
3) Our proposed SoS and LMI-based RoS and its volume estimation, enables the estimation of CCT (the time within which a fault must be cleared to retain stability, providing a practical time-margin for stability) by way of post-fault simulation to determine the time when the operating point crosses the boundary of the estimated RoS, which we have also implemented. This provides an alternate means of characterizing CCT in contrast to the controlling unstable equilibrium point (CUEP)-based method [24].
4) We introduce and implement a new quadratic-constrained-quadratic-program (QCQP)-based precise computation of RM of a fault, which is the margin to false-tripping of a nondesignated relay due to the swings/transients arising after clearance of a fault by the designated relay. The notion of RM was introduced in [25] and is equivalent to the fault norm in [26] and the severe contingency indicator (SCI) in [27].
5) We introduce the *security as well as stability* informed notions of LSM and LL to account for: a) the available margin for load increment prior to violation of any of the security or stability constraints and b) the required load shedding, when such margin is negative. We extend the continuation power flow (CPF) [28] to implement computation of these two measures.
6) We implement all the above methods in MATLAB and illustrate with respect to three 7-bus test systems differing from each other only in the locations of generators, against all possible length-2 contingencies (a total of 582 cases). To further validate the proposed framework, we implemented it on the IEEE 30-bus test system and computed its resilience measures with respect to all faults (a total of 73 cases).

A. Related Works

A literature search reveals a few prior works on resilience quantification in the domain of power systems. Kinney *et al.* [29] suggested measuring the damage of occurrence of a fault in form of the loss of average normalized grid efficiency, where the efficiency of distribution between substation i to j is defined as the harmonic composition of efficiency of the edges along the most efficient path connecting i and j. Maliszewski and Perrings [30] defined the resilience of a power system using two factors: 1) the available infrastructure, the biophysical environment and their interaction and 2) priority of restoration to the utility company and their expected response time. Francis and Bekera [31] introduced the notion of an uncertainty-weighted resilience measure involving absorptive capacity, adaptive capacity and recovery, and restorative capacity. A system-level measure to quantify the resilience of smart grid is also proposed in [32], which integrates five indices: 1) expected hazard frequency; 2) initial failure scale; 3) maximum impact level; 4) RT; and 5) recovery cost. To facilitate planning, design, investment, and operation of energy systems, [33] formulates a resilience matrix, where each entry of the matrix correlates how a system's ability to [plan/prepare, absorb, recover, and adapt] to an energy-related change can be improved by measures taken in the [physical, information, cognitive, and social] domain. Willis and Loa [34] summarized resilience measures of energy distribution systems, where the metrics are: inputs available to support resilience, capacity to organize those inputs to support resilience, capabilities of what tasks can be performed,apparent impedance seen and the performance and outcomes that describe what is produced by an engineered system. Arghandeh *et al.* [35] *qualitatively* discusses resilience of a power system and contrasts it from the related notions of

stability, robustness, and reliability; no formal *quantification* of resilience is provided. Panteli *et al.* [9] proposed quantification of decline in the resilience level of a power system under a given sequence of events by the time-integral of LL, which is a function of LL and recovery-time, and hence, is also captured in our framework. A time-integral-based method is also used in [10] for quantifying resilience of energy and water distribution systems, modeling their interdependency. Soman *et al.* [27] considered an indirect way of assessing transient stability against a fault by way of measuring the angle trajectory sensitivity with respect to a line impedance (following a fault); the sensitivity becomes higher as the operating point gets closer to the boundary of RoS. Other indirect measures of transient stability that have been examined in the literature include: RM and RSM [25] that are computed based on the apparent impedance seen by a relay [27]. We do examine an indirect measure of transient stability, namely, CCT, as defined in Section III. In addition, we also employ a direct quantification of the TSM in form of an inner approximation of the volume of the RoS (of the post-clearance subsystem).

The notion of resilience has also been explored outside power systems. Filippini and Silva [36] provided a general modeling framework to represent the interdependent modern infrastructures in order to support reasoning of system vulnerabilities and overall resilience. Fujita *et al.* [37] proposed an approach that allows integration of the state-of-the-art solutions of "granular computing" into different phases of resilience analysis of critical infrastructures. Zeng *et al.* [38] suggested the ability of a cyberphysical network to recover from cascading failures caused by an adversarial attack, to be a key measure of resilience and explores network topology designs to determine the tradeoff between resilience versus operational efficiency.

II. Preliminaries

$\mathbb{R}$ (resp., $\mathbb{R}_{\geq 0}$ and $\mathbb{R}_{+}$) denotes the space of all real (resp., non-negative real and positive real) scalars. $\mathbb{R}^n$ denotes the space of real vectors of dimension n. For any $x \in \mathbb{R}^n$ and $p \geq 1$, $||x||_p$ denotes the p-norm of x.

A. Power System Model

In order to present our approach of computing various resilience measures, we employ the classical power system model, described next. When a power system comprising of M buses and N generators, is at an equilibrium (so the dynamical variables are constant at their equilibrium values), one solves a set of algebraic power flow equations to obtain the values of the unknown variables (generator bus voltage angle and reactive power, load bus voltage phasor, slack bus active, and reactive powers) given the values for the known ones (generator bus voltage magnitude and active power, load bus active and reactive powers, slack bus voltage phasor). For each bus i in the system, letting P_{Gi}, Q_{Gi}, P_{Li}, Q_{Li}, V_i, and δ_i denote, respectively, the injected active power, injected reactive power, load active power, load reactive power, bus voltage magnitude, and its angle (measured relative to the slack bus voltage angle), the power flow equations for the bus $i \in \{1, \ldots, M\}$ are given by

$$P_{Gi} = \sum_{j=1}^{M} V_i V_j Y_{ij} \cos\big(\theta_{ij} - \delta_i + \delta_j\big) + P_{Li}$$
$$Q_{Gi} = \sum_{j=1}^{M} V_i V_j Y_{ij} \sin\big(\theta_{ij} - \delta_i + \delta_j\big) + Q_{Li} \tag{1}$$

where $Y_{ij}\angle\theta_{ij}$ denotes the (i, j)th element of the bus admittance matrix. Knowing the values $V_i\angle\delta_i$ from the solution of the above power flow equations (typically solved by Newton–Raphson's method), one can also compute the generator q-axis voltage phasor denoted by $E_i\angle\delta_i'$ for the generator i connected to bus i using the following equation for $i \in \{1, \ldots, N\}$:

$$E_i\angle\delta_i' = V_i\angle\delta_i + z_i \sum_{j=1}^{M} Y_{ij}\angle\theta_{ij}\big(V_i\angle\delta_i - V_j\angle\delta_j\big) \tag{2}$$

where z_i denotes the direct-axis transient impedance of the generator i. The above power flow equations can be rewritten in Kron-reduced form that absorbs the generator transient impedances, elements of bus admittance matrix, and the load admittance into a single reduced admittance matrix, and is given as below for $i \in \{1, \ldots, N\}$

$$P_{Gi} = \sum_{j=1}^{N} E_i E_j Y'_{ij} \cos\Big(\theta'_{ij} - \delta'_i + \delta'_j\Big)$$
$$Q_{Gi} = \sum_{j=1}^{N} E_i E_j Y'_{ij} \sin\Big(\theta'_{ij} - \delta'_i + \delta'_j\Big) \tag{3}$$

where $Y'_{ij}\angle\theta'_{ij}$ denotes the (i, j)th element of the Kron-reduced admittance matrix.

For the transient stability analysis, each generator is modeled by the classical swing equation, which for the generator $i \in \{1, \ldots, N\}$ is given by:

$$\dot{\delta}'_{i,N} = \omega_i - \omega_N \tag{4}$$
$$M_i\dot{\omega}_i + D_i\omega_i + P_{Gi} = P_{mi} \tag{5}$$

where for the ith generator, M_i, D_i, P_{mi} are constants denoting inertia, damping, and mechanical power input, ω_i denotes the speed and $\delta'_{i,N}$ denotes the q-axis voltage angle relative to that of the Nth generator considered as the reference. P_{mi} equals the sum of $D_i\omega_i$ and P_{Gi} evaluated at the equilibrium, which can be seen by setting the derivative term to zero in (5). During transients, however, $\delta'_{i,N}$, ω_i and P_{Gi} in (5) are dynamic variables, where as implied by (3), their variability is triggered by a change in the admittance matrix $Y'\angle\theta'$ caused by occurrence of a fault. E_is in (3) are held constant at their prefault equilibrium values.

B. Fault Models and Our Notions of Resilience Measures

Power systems are subject to various faults/attacks that ultimately affect the generation, the transformers, the loads and the admittance matrix (that may also correspond to islanding). Even the cyber faults/attacks ultimately cause malfunction of the physical components, namely, generators, loads, transformers, and lines/buses, which is what we capture. Once

a fault occurs in any component, the faulty component is disconnected from the rest of the system by action of protective relay, which we refer as *fault clearance*; the subsequent restoration of the component is referred as *recovery/repair* interchangeably.

For a given power system, let F be the set of faults of interest. For a positive integer l, we use F^l to denote the set of all faults-sequences of length l (i.e., containing l faults). Note that l can be chosen based on the contingency level of interest (e.g., for $N-3$ contingency level, choose $l=3$), and in general, we will assess the system status following a sequence of faults that are still "active," i.e., the ones that have not yet been repaired. For a fault-sequence $\phi \in F^l$, we use $\phi(k)$ to denote the length-k prefix of ϕ. The notation $I_{\phi(k)}$ is used to denote the set of all islanded subsystems of the original system, resulting from the occurrence and clearance of the fault-sequence prefix $\phi(k)$, while the initial system is denoted by I_0. A subsystem is "live" if it contains at least one generator and a load, and the set of all such live subsystems is denoted by $\mathcal{I}_L$. For each islanded subsystem $r \in I_{\phi(k)}$, we compute its six different measures of resilience: TSM, CCT, RM, LSM, LL, and RT. These are then normalized (to take a non-negative value of at most 1) and averaged (across all fault-sequences using their occurrence probabilities) to form an overall measure of resilience level of a power system. The detailed mathematical formalizations are presented in Sections III–IV.

III. Resilience Measures wrt Sequence of Faults

In this section, we present our proposed definitions and computation methods for the six atomic resilience measures: TSM, CCT, RM, LSM, LL, and RT, with respect to a single prefix of a fault-sequence. Our approach to aggregate those over a fault-sequence and finally, computing their normalized and averaged values over the set of all possible (active) fault-sequences of a given length, is presented in Section IV.

A. Transient Stability Margin

For a power system with dynamics defined by (4) and (5), the state vector consists of the $N-1$ relative angles (excluding that of the reference generator with zero relative angle) and the N absolute speeds of the generators, denoted as $x \in \mathbb{R}^{2N-1}$, and its nonlinear dynamics may be viewed as a state equation

$$\dot{x} = f(x) \tag{6}$$

where $f : \mathbb{R}^{2N-1} \to \mathbb{R}^{2N-1}$ is a locally Lipschitz nonlinear map defined over a domain $D \subseteq \mathbb{R}^{2N-1}$. $x_0 \in \mathbb{R}^{2N-1}$ is an equilibrium point if there is no rate of change at that state, i.e., if $f(x_0) = 0$.

Definition 1 [39]: For an autonomous system defined by (6), its RoS corresponding to its equilibrium x_0 is the largest set $\Omega \subseteq D$ containing x_0, such that if the system starts at any state in Ω, it eventually reaches x_0 and remains there. An equilibrium state, whose corresponding RoS has nonempty interior, is called a stable equilibrium point (SEP).

When a stable power system is perturbed due to occurrence of a fault (resp., a transient disturbance), the operating point after clearance of the fault (resp., withdrawal of the cause of disturbance), must lie within the RoS corresponding to the post-clearance (resp., post-withdrawal) SEP, for the post-clearance (resp., post-withdrawal) system to eventually reach the SEP. Hence the TSM of a power system, against occurrence of a fault (resp., a disturbance), can be directly measured by the size of the RoS corresponding to the SEP of the post-clearance (resp., post-withdrawal) system.

The RoS of a system can be expressed as a sublevel set $\{x : V(x) \le c\}$ of a Lyapunov function $V(x)$ for a level value $c \in \mathbb{R}_+$. For a given c, $V(x)$ can be found as the solution of the following optimization problem [13], [40]:

$$\begin{aligned} &\underset{V \in \mathbb{P}_{x,+}}{\text{maximize}} \quad \gamma \\ &\text{subject to:} \\ &\left\{x \in \mathbb{R}^{2N-2} | V(x) \le c, \dot{V}(x) \ge 0, x \ne 0\right\} = \varnothing \\ &\left\{x \in \mathbb{R}^{2N-2} | p_+(x) \le \gamma, V(x) \ge c\right\} = \varnothing \end{aligned} \tag{7}$$

where γ is a scalar, $\mathbb{P}_{x,+}$ denotes the space of all polynomials defined over indeterminate x with real coefficients, which are evaluated positive for all x except the origin where those are zero, and $p_+(x) \in \mathbb{P}_{x,+}$ is a user-defined polynomial that sets a lower bound for the desired sublevel set. Note $\dot{V}(x) = (dV/dx)(dx/dt) = (dV/dx)f(x)$, and so the solution does depend on the system dynamics $f(\cdot)$.

If the emptiness constraints in (7) are made of polynomial functions, those can be formulated as a semi-definite program involving SoS polynomials, applying the *Positivstellensatz* theorem [41]. Although the power system dynamics involves trigonometric functions, it turns out that those can be transformed into polynomials through a change of variables from x to $z \in \mathbb{R}^{3N-2}$ as follows [14]. For each $i \in \{1, \ldots, N-1\}$, we define a triplet of variables

$$z_{3i-2} = \sin \delta'_{i,N}, z_{3i-1} = \omega_i, z_{3i} = 1 - \cos \delta'_{i,N} \tag{8}$$

and $z_{3N-2} = \omega_N$ is added to those. Following the change of variables since the constraints in (7) involve only polynomial functions, one can obtain the following SoS version of (7) using Positivstellensatz theorem [11], [41] (see Appendixes A and B of the extended version of this article [42] for more details and a numerical example):

$$\begin{aligned} &\underset{V \in \mathbb{P}_{z,+}, v_1, v_2 \in \mathbb{P}_z^{N-1}, s_1, s_2, s_3 \in \mathbb{S}_z}{\text{maximize}} \quad \gamma \\ &\text{subject to:} \\ &-s_1(z)(c - V(z)) - s_2(z)\dot{V}(z) - v_1^T(z)g(z) - q_+(z) \in \mathbb{S}_z \\ &-s_3(z)(\gamma - p_+(z)) - v_2^T(z)g(z) - (V(z) - c) \in \mathbb{S}_z \end{aligned} \tag{9}$$

where $q_+(z) \in \mathbb{P}_{z,+}$ is user selected, $\mathbb{P}_z$ denotes the space of all polynomials defined over indeterminate z with real coefficients, $\mathbb{P}_z^{N-1}$ denotes the $N-1$ dimensional real vector with each of its elements in $\mathbb{P}_z$, and $\mathbb{S}_z \subseteq \mathbb{P}_z$ denotes the space of all SoS polynomials defined over z.

Due to presence of the product of polynomial variables in the first two terms of the last constraint, the optimization problem in (9) is nonconvex, in general. An iterative algorithm to find a local optimal solution of (9) is provided in [13] with its proof of convergence; our recent work in [40] provides further computational enhancement.

If the search for Lyapunov function $V(z)$ is restricted to the set of degree-2 polynomials in the space $\mathbb{P}_{z,+} \cap \mathbb{S}_z$, the computed RoS $V(z) \leq c$ defines an ellipsoid $\mathcal{E}$ expressed as follows:

$$\mathcal{E} := \left\{ z \in \mathbb{R}^{3N-2} | z^T A z + 2b^T z \leq c \right\} \tag{10}$$

where $A \in \mathbb{R}^{(3N-2)\times(3N-2)}$ is symmetric positive semidefinite, $b \in \mathbb{R}^{3N-2}$, and both A and b are obtained from the coefficients of the already computed $V(z)$. Here, we present our formulation of computing the volume of an ellipsoid defined by (10), by parametrizing it as the image of the unit Euclidean ball under an affine transformation, as follows:

$$\mathcal{E} = \{ Bz + d | \|z\|_2 \leq 1 \} \tag{11}$$

where $B \in \mathbb{R}^{(3N-2)\times(3N-2)}$ is symmetric positive semidefinite and $d \in \mathbb{R}^{3N-2}$. One can obtain the parameters B and d of (11) by solving the following convex problem, in which κ is a scalar [15]:

$$\begin{aligned} &\underset{B,d,\kappa}{\text{minimize}} \log\det\left(B^{-1}\right) \\ &\text{subject to:} \\ &\begin{bmatrix} -\kappa + c + b^T A^{-1} b & 0 & \left(d + A^{-1}b\right)^T \\ 0 & \kappa & B \\ d + A^{-1}b & B & A^{-1} \end{bmatrix} \succeq 0. \end{aligned} \tag{12}$$

Equation (12) is a semidefinite program that can be solved efficiently (complexity is polynomial wrt N) by interior-point method.

Note the transformation of $\mathcal{E}$ from (10) to (11), can be viewed as one of the computation of a maximal volume ellipsoid inscribed in an (intersection of multiple) ellipsoid(s) [15]. The volume of $\mathcal{E}$ denoted by $\mathcal{V}$ is computed by

$$\mathcal{V} = \det(B) \times \mathcal{V}_u \tag{13}$$

where $\mathcal{V}_u$ denotes the volume of the unit Euclidean ball in $\mathbb{R}^{3N-2}$, and $\det(B)$ denotes the determinant of B. There exists a closed form expression for $\mathcal{V}_u$ in literature, but since $\mathcal{V}_u$ is just a constant for the state spaces of identical dimension, it suffices to consider $\det(B)$ for comparing two systems of identical state-space dimension.

Definition 2: The TSM of a subsystem $r \in I_{\phi(k)}$, following the occurrence and clearance of the length-k fault-sequence $\phi(k) \in F^k$ is defined as follows:

$$\text{TSM}_{\phi(k),r} := \left(\mathcal{V}_{\phi(k),r}\right)^{1/3N-2} \tag{14}$$

where $\mathcal{V}_{\phi(k),r}$ denotes the volume of the estimated RoS corresponding to the SEP of the subsystem $r \in I_{\phi(k)}$.

Note when an islanded subsystem has no generator or no load, there is zero stability-margin, i.e., $\mathcal{V}_{\phi(k),r} = 0$ whenever $r \notin \mathcal{I}_L$. On the other hand, when an island contains load and only a single generator, its classical model becomes linear with the whole state space being its RoS, i.e., $\mathcal{V}_{\phi(k),r} = \infty$.

B. Critical Clearance Time

The CCT represents the maximum time window, within which a fault must be cleared after its occurrence in order to ensure stability of the post-clearance system. After a fault occurs at time t_0 in a power system operating at a SEP, say x_0, the system dynamics changes due to the change in the transfer admittance. If the fault is cleared by removing the faulty component at time t_c, the system dynamics changes again with an associated RoS, say Ω. Then by *Definition 1*, the stability of the post-clearance system is eventually restored if and only if the operating point $x(t_c) \in \Omega$. Hence, the CCT of a fault can be defined as the time elapsed from occurrence of the fault, until the post-fault system trajectory reaches the boundary of Ω. It also follows that if the fault clearance time $t_c - t_0$ is more than the CCT, the post-clearance system can never eventually reach the desired post-clearance equilibrium. For a subsystem r formed after clearance of a fault $f \in F$, we can obtain a conservative estimate of its CCT, as the crossing time of the boundary of the inner approximation of post-clearance RoS [obtained solving (9)] as follows:

$$\text{CCT}_{f,r} := \text{argmax}_t \{ V(x(t)) | V(x(t)) \leq c, x(t_0) = x_0 \} \tag{15}$$

where $x(t)$ evolves in time following the post-fault dynamics.

Since a generator outage does not leave any faulty component in the system, the corresponding CCT is ∞, i.e., $\text{CCT}_{f,r} = \infty$ when f is outage of a generator. In case of a line (resp. transformer) fault, the post-fault system trajectory depends on the exact location of the fault on the line (resp. transformer). So a worst-case fault location with smallest possible CCT is identified through a discretized search over the possible fault locations along the line (resp. transformer).

Definition 3: For a subsystem $r \in I_{\phi(k)}$ resulting from the length-k fault-sequence $\phi(k) \in F^k$, its resilience measure CCT is defined as follows:

$$\text{CCT}_{\phi(k),r} := \text{CCT}_{f,r} \tag{16}$$

where $f \in F$ is the last fault in the fault-sequence $\phi(k) \in F^k$.

C. Relay Margin

Each component of a power system is equipped with designated protective relay(s) meant to monitor and respond to a possible fault in that component. Every relay has a predetermined operating zone, and when the value of the variable monitored by the relay enters into its operating zone, and remains inside the zone for a predetermined time, the relay sends a "tripping" signal for clearance of the component. Such clearance of a faulty component causes change in the overall system dynamics that leads to transient swings across the system. Such transient swings of the variables can cause the nondesignated relays to trip, even though their corresponding protected components are healthy, which is referred as *false-tripping*. False-tripping of a relay results in an undue outage in a system, thus (possibly) degrading the quality-of-performance in terms of undesired loss of generation and/or load. We measure the degree of robustness to such false-tripping by the RM [25].

A relay protecting a line, diagnoses a fault in the line by checking if the impedance seen (i.e., the instantaneous ratio of voltage and current phasors) remains inside its operating circle (the "Mho" circle) for a specified duration. The

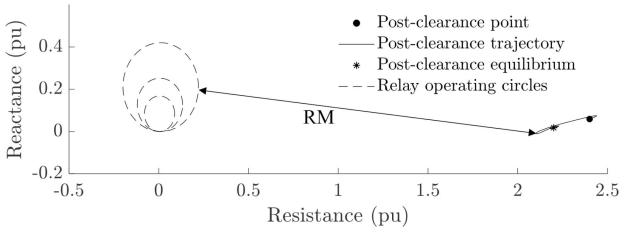

Fig. 1. Impedance trajectory seen by *Line 7-6* distance relay placed near *Bus 7*, after clearance of fault in *Line 7-4* at 60 ms (for PS_1).

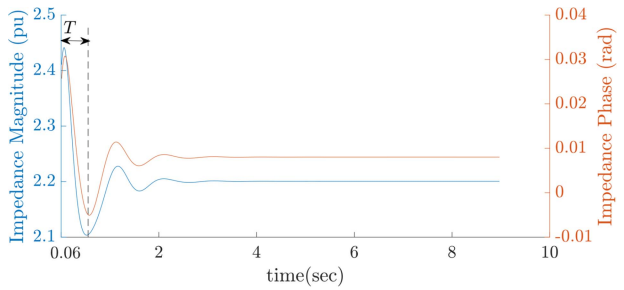

Fig. 2. Impedance magnitude and phase seen by *Line 7-6* distance relay placed near *Bus 7*, after clearance of fault in *Line 7-4* at 60 ms (for PS_1).

minimum distance between the post-clearance impedance trajectory to the relay operating circle is defined as its RM. While there exist multiple operating circles (typically zone 1, 2, and 3) for a relay, we measure RM with respect to the largest one (i.e., zone 3) to account for the maximum possible number of false-interventions. Note since the relays used for protecting the buses and transformers are of differential nature, the effect of transient swing is cancelled in the differential variable monitored by them. Hence, these relays are not vulnerable to post-clearance transient swing (i.e., $\mathrm{RM} = \infty$).

For illustration, consider a fault in *Line 7-4* of the system PS_1 of Fig. 4(a), which gets cleared in 60 ms. Fig. 1 shows the post-clearance impedance trajectory seen by the distance relay installed for *Line 7-6* near *Bus 7*, where the RM is also depicted. Fig. 2 shows the trajectories of the post-clearance magnitude and phase of the impedance seen by that relay. Since the trajectories are damped periodic, the minimum distance of the post-clearance transient swing to the relay operating circle is realized inside the first cycle, denoted by T as shown in Fig. 2.

Let $Z_{f,i}[0, T]$ denote the trajectory of impedance over the interval $[0, T]$ seen by the distance relay i (installed near one of the adjacent buses of a nonfaulty line), following clearance of the fault $f \in F$. Accordingly, RM corresponding to the fault $f \in F$ for that distance relay can be computed as follows:

$$\mathrm{RM}_{f,i} = \underset{x:\|x-c\|_2 \le r, y \in Z_{f,i}[0,T]}{\text{minimize}} \|x - y\|_2 \tag{17}$$

where c and r are two scalars denoting the center and radius of the outermost relay operating circle, respectively. T can be numerically computed as the time elapsed after fault-clearance, until the second inflection along the impedance trajectory is encountered. Then (17) can be solved by solving a set of

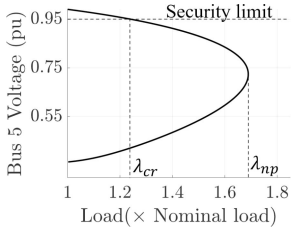

Fig. 3. Steady state variation of Bus 5 voltage of PS_1 with increase in load from nominal value ($\lambda = 1$).

QCQP, formed by fixing y at the respective discrete samples from $Z_{f,i}[0, T]$, and picking the minimum of the solution set.

Definition 4: For a subsystem $r \in I_{\phi(k)}$ containing a set of distance relays denoted $\mathcal{D}$, resulting from the length-k fault-sequence $\phi(k) \in F^k$, its resilience measure RM is defined as follows:

$$\mathrm{RM}_{\phi(k),r} := \min_{i \in \mathcal{D}} \mathrm{RM}_{f,i} \tag{18}$$

where $f \in F$ is the last fault in the fault-sequence $\phi(k) \in F^k$.

D. Load Loss and Load Security Margin

In [6], we considered LL (denoted as LoPr in [6]) as a resilience measure, but the concept of LL was limited only to the loss of load due to disconnection caused by fault-clearance(s), which is named *consequential* LL [4], in practice. In a practical power system, however, LL can also take place if any of the security limits is violated, even though there is no disconnection. The power system security limits are usually determined based on the admissible steady state ranges of the power flow variables: 1) magnitude of bus voltages; 2) loading of the respective lines and transformers; and 3) generated active and reactive powers. We refer to these algebraic variables as the security variables.

Loads can slowly vary throughout the operation of a power system. Such variation of load causes the SEP to drift from its nominal value. A typical variation of the equilibrium value of the voltage of *Bus 5* of the system PS_1 of Fig. 4(a) due to increase of the loads from its nominal unit value, is shown in Fig. 3 (note similar curves can also be drawn for any of the other security variables). The nose-point (also called the bifurcation point) of the curve in Fig. 3, corresponds to the maximum load (denoted λ_{np} in Fig. 3) for which a solution of the power flow equations (1) exists. There exists a smaller upper limit to load (denoted λ_{cr} in Fig. 3) referred as the "critical load," beyond which one or more of the security variables violate their limit. In general, the critical load is smaller than the noise-point load, and it is the critical load that we use to determine the LSM.

After clearing a fault, it is important that the post-clearance load remains below the critical limit, so that the steady state values of the security variables lie within their respective limits. We call the margin to the critical load with respect to the nominal load, the LSM. For example in Fig. 3, the system must be operated at load below its critical value of approximately 1.26 times the nominal load, to restrict the bus voltage in its security interval [0.95, 1.05] pu. So the LSM in this case, is no

more than 0.26 times the nominal load. Note a power system is aided with various controls to ensure secure operation, such as switched capacitors, LTC operation, SVC, synchronous condenser, generator field voltage adjustment, etc., and the LSM is computed under the best-case control scenario. Also note that when the LSM is negative, one must accept load shutdowns, incurring certain LL.

For computation of both LL and LSM, we adopt the well-known method of CPF [28] that provides a systematic way to compute the steady state effects of load variation on the power flow variables. In CPF, the variation of load (and the associated adjustment of generation), are parametrized by $\lambda \in \mathbb{R}_{\geq 0}$, where $\lambda = 1$ corresponds to the nominal load and generation. For this setting, the power flow equations (1) are written as

$$\lambda P_{Gi0} = \sum_{j=1}^{M} V_i V_j Y_{ij} \cos\big(\theta_{ij} - \delta_i + \delta_j\big) + \lambda P_{Li0} \tag{19}$$

$$Q_{Gi} = \sum_{j=1}^{M} V_i V_j Y_{ij} \sin\big(\theta_{ij} - \delta_i + \delta_j\big) + \lambda Q_{Li0} \tag{20}$$

where P_{Gi0}, P_{Li0}, and Q_{Li0} denote the nominal values of P_{Gi}, P_{Li}, and Q_{Li}, respectively. Note (19) and (20) utilize an even-participation of all the generators and loads. The extension to a more general case is straightforward.

Let $L_{\phi(k),r}$ be the active power consumed by the loads originally connected to the subsystem $r \in I_{\phi(k)}$. The notation $\lambda_{\phi(k),r}$ is introduced to denote the critical load (i.e., minimum value of λ for which one or more of the security variables violate their limit) of the subsystem $r \in I_{\phi(k)}$. Note when $\lambda_{\phi(k),r} > 1$, there is positive LSM, but when $\lambda_{\phi(k),r} < 1$, some LL must be incurred. Using the critical load parameter $\lambda_{\phi(k),r}$, we define the two resilience measures LL and LSM.

Definition 5: The LL incurred within the subsystem $r \in I_{\phi(k)}$ is given by

$$\mathrm{LL}_{\phi(k),r} \coloneqq -L_{\phi(k),r} \times \min\big(0, \lambda_{\phi(k),r} - 1\big) \tag{21}$$

whereas, its LSM is given by

$$\mathrm{LSM}_{\phi(k),r} \coloneqq L_{\phi(k),r} \times \max\big(0, \lambda_{\phi(k),r} - 1\big) \tag{22}$$

where as noted above $\lambda_{\phi(k),r}$ is the critical load for the subsystem $r \in I_{\phi(k)}$, and $L_{\phi(k),r}$ is the active power of the loads originally connected to the subsystem $r \in I_{\phi(k)}$.

Note both LSM and LL are defined in terms of only the active powers since the reactive powers essentially add to system's internal losses that are harder to measure in practice.

E. Recovery Time

The RT also serves as another resilience measure. It is the time an operator is expected to take to restore the system to its prefault normalcy. Aside from the fault-sequence, the RT depends on other factors, such as geographic location, availability of crew, supporting infrastructure readiness, weather condition, etc., [43]–[45]. Chow *et al.* [43] analyzed the statistical significance of various factors that affect the RT. Rodriguez and Vargas [44] proposed a fuzzy-logic-based technique to estimate RT, where the relative significance of different factors is set by the user. Jaech *et al.* [45] studied the estimation of RT distribution, a gamma distribution with parameters dependent on the aforementioned factors, by employing a multilayer neural net for training against the historical records. Such techniques involving historical data and statistical estimation may be used to forecast the time needed to recover from the faults.

For any fault $f \in F$, let $\bar{f}$ denote its recovery action and $\bar{F}$ denotes the set of all such recovery actions. Also let $A \coloneqq F \cup \bar{F}$ denote the set of all fault and recovery actions, and $\Psi \subseteq (A \times \mathbb{R}_+)^l$ denote the set of all "feasible" timed-sequences of a total of l faults and recovery actions, where each element of a timed-sequence consists of a fault/recovery action tagged with its occurrence/completion time, formally defined as

$$\begin{aligned}\Psi \coloneqq \Big\{\psi = \Big(\Big(a_1^\psi, t_1^\psi\Big), \ldots, \Big(a_l^\psi, t_l^\psi\Big)\Big) \in (A \times \mathbb{R}_+)^l \,|\, \\ \forall k \leq l : t_k^\psi > t_{k-1}^\psi \\ a_k^\psi = \bar{f} \Rightarrow \#(f, \psi(k)) \geq \#\big(\bar{f}, \psi(k)\big)\Big\}\end{aligned} \tag{23}$$

where $\psi(k)$ denotes the length-k prefix of fault-repair sequence $\psi \in \Psi$, and $\#(f, \psi(k))$ (resp. $\#(\bar{f}, \psi(k))$) denotes the total number of faults (resp. recoveries) in the sequence $\psi(k)$. The condition $\#(f, \psi(k)) \geq \#(\bar{f}, \psi(k))$ simply captures the fact that for a repair action to occur, a corresponding fault must occur first.

For a sequence of first k faults $\phi(k) \in F^k$ (with the corresponding sequence of recovery actions $\bar{\phi}(k)$) in the timed-sequence ψ, its RT is obtained as the difference between the latest repair action in $\bar{\phi}(k)$ versus the earliest fault action in $\phi(k)$

$$\begin{aligned}\mathrm{RT}_{\psi,\phi(k)} \coloneqq \max_{i \in \{1,\ldots,k\}} \Big\{t_i^\psi \,|\, a_i^\psi \in \bar{\phi}(k)\Big\} \\ - \min_{j \in \{1,\ldots,k\}} \Big\{t_j^\psi \,|\, a_j^\psi \in \phi(k)\Big\}.\end{aligned} \tag{24}$$

The average RT for a length-k fault-sequence $\phi(k) \in F^k$ is then given by

$$\mathrm{RT}_{\phi(k)} = \sum_{\psi \in \Psi_{\phi(k)}} p_\psi . \mathrm{RT}_{\psi,\phi(k)} \tag{25}$$

where $\Psi_{\phi(k)} \subseteq \Psi$ is the set of all timed-sequences containing $\phi(k)$ fault-sequence prefix, and $p_\psi \in [0, 1]$ denotes the probability of $\psi \in \Psi_{\phi(k)}$. Note the recovery is a property of only the active fault-sequence and *all* the islanded subsystems formed by it, i.e., it does not depend on any individual subsystem, and hence it is *not* subscripted by the index of a subsystem, unlike the other resilience measures introduced earlier in this section.

IV. Resilience Indices: Normalized and Averaged wrt All Fault-Sequences

In last section, we introduced the six resilience measures $\mathrm{TSM}_{\phi(k),r}$, $\mathrm{CCT}_{\phi(k),r}$, $\mathrm{RM}_{\phi(k),r}$, $\mathrm{LSM}_{\phi(k),r}$, $\mathrm{LL}_{\phi(k),r}$, and $\mathrm{RT}_{\phi(k)}$, where $\phi(k)$ is the length-k prefix of an active fault-sequence $\phi \in F^l$, and $r \in I_{\phi(k)}$ is an islanded subsystem resulting from the occurrence of the fault-sequence $\phi(k)$. Next, we define their respective aggregated values following

an entire fault-sequence $\phi \in F^l$. This is done by choosing the minimum value (for TSM, CCT, and RM) across all resulting islands of all the prefix fault-sequences: $r \in I_{\phi(k)} \forall k \leq l$, or by choosing the value of the total (for LSM, LL, and RT) across all resulting islands $r \in I_{\phi(l)}$, upon the entire fault-sequence.

Definition 6: The aggregate resilience measures TSM_ϕ, CCT_ϕ, RM_ϕ, LSM_ϕ, LL_ϕ, and RT_ϕ following a fault-sequence $\phi \in F^l$, are defined as:

$$\begin{aligned}
\text{TSM}_\phi &:= \min_{k\leq l, r\in I_{\phi(k)}} \text{TSM}_{\phi(k),r} \\
\text{CCT}_\phi &:= \min_{k\leq l, r\in I_{\phi(k)}} \text{CCT}_{\phi(k),r} \\
\text{RM}_\phi &:= \min_{k\leq l, r\in I_{\phi(k)}} \text{RM}_{\phi(k),r} \\
\text{LSM}_\phi &:= \sum_{r\in I_{\phi(l)}} \text{LSM}_{\phi(l),r} \\
\text{LL}_\phi &:= \sum_{r\in I_{\phi(l)}} \text{LL}_{\phi(l),r} \\
\text{RT}_\phi &:= \text{RT}_{\phi(l)}.
\end{aligned} \tag{26}$$

The six aggregated measures introduced in Definition 6 possess their own units, and to be able to compare them against each other, we propose a normalization of each resilience measure against the range of its computed values to obtain a normalized value in the interval [0,1], where 1 (resp., 0) means a 100% (resp., 0%) level for that measure. In doing the normalization, a type of scaling, it is practical to have a higher resolution at the lower values of a measure than at its higher values (a type of diminishing returns), and accordingly a nonlinear normalization is more practical. In fact, any concave monotonic increasing nonlinear mapping that maps the range of values taken by a resilience measure to the unit interval, can be used for normalization. Since the different resilience measures range over different supports, it is also desirable that the normalization be invariant with respect to scaling of the support (whenever it is finite). We adopt the following normalization possessing the aforementioned properties.

Definition 7: Given any resilience measure V with its computed values in the range $[V_{\min}, V_{\max}]$, the normalized value of $V \in [V_{\min}, V_{\max}]$ denoted $nV \in [0, 1]$, is defined by the function

$$nV := \begin{cases} 1 - e^{-\alpha(V-V_{\min})}, & V_{\max} = \infty \\ 1 - e^{-[\frac{\alpha}{V_{\max}-V}](V-V_{\min})}, & V_{\max} < \infty \end{cases} \tag{27}$$

where $\alpha > 0$ is a user-selected parameter. Normalization of each of the six resilience measures of Definition 6, obtained using the formula (27), yields the corresponding normalized resilience measures, denoted by $nTSM_\phi$, $nCCT_\phi$, nRM_ϕ, $nLSM_\phi$, nLL_ϕ, and nRT_ϕ, respectively.

Note the above formula of (27) is simply an exponential saturation from 0 to 1, over the interval $[V_{\min}, V_{\max}]$. If a resilience measure has unbounded support [first case in (27)], the rate-constant is simply the user selected parameter α. On the other hand, if the support is finite [second case in (27)], the rate is variable and progressively increasing causing the saturation to occur within the finite support (akin for example to the tangent function, which also has a variable growth rate that is progressively increasing).

Note the second formula of (27), used for the normalization of a resilience measure possessing a finite support, has the desirable property that if the support $[V_{\min}, V_{\max}]$ as well as a value $V \in [V_{\min}, V_{\max}]$ are scaled identically, the normalized value nV remains unaltered. In this sense, the normalization is *scale-invariant*. To see this, define fV as the fractional value of $V \in [V_{\min}, V_{\max}]$ relative to its support as the ratio of its distance to $V_{\min}$ to the distance of $V_{\max}$ to $V_{\min}$

$$fV := \frac{V - V_{\min}}{V_{\max} - V_{\min}}. \tag{28}$$

Then the second case in (27) can be rewritten as

$$nV := 1 - e^{-\alpha \frac{fV}{1-fV}} \tag{29}$$

which indicates that the normalization value remains the same if the fractional value does not change. The latter is the case if there is an identical scaling of V relative to $V_{\min}$ (i.e., of $V - V_{\min}$) as well as the support $[V_{\min}, V_{\max}]$, and the scaling factor in the numerator and the denominator of (28) cancel each other, preserving the value of fV.

Definition 7 formalizes the 6 aggregate resilience measures for each given fault-sequence $\phi \in F^l$. Next, we propose to compute their averages across all possible fault-sequences of a desired length, against their occurrence probabilities, in order to obtain the set of 6 overall resilience indices of a given power system (note the fault-sequence length will be chosen as l if interested in evaluating resilience of a given power system against $N - l$ level contingencies). The occurrence-probability of a fault-sequence is simply the product of the occurrence probabilities of the individual faults in the sequence, and those can be obtained from the historical records. For $f \in F$, letting $p_f \in [0, 1]$ denote its occurrence probability such that $\sum_{f\in F} p_f = 1$, we can compute the occurrence probability p_ϕ of each active fault-sequence $\phi \in F^l$ as $\prod_{1\leq k\leq l} p_{f(k)}$, where $p_{f(k)}$ denotes the occurrence probability of the kth fault $f(k) \in F$ of the fault-sequence ϕ. Averaging each of the 6 normalized resilience measures with respect to the occurrence probabilities of the fault-sequences, yields an overall resilience measure, a set of 6 indices for a power system as summarized as follows.

Definition 8: The overall resilience measure $R_l \in [0, 1]^6$ of a given power system with respect to all possible fault-sequences of a certain length $l > 0$ is given by

$$\begin{aligned}
R_l := \sum_{\phi\in F^l} p_\phi \big[& nTSM_\phi \;\; nCCT_\phi \;\; nRM_\phi \;\; nLSM_\phi \\
& (1 - nLL_\phi) \;\; (1 - nRT_\phi) \big]^T
\end{aligned} \tag{30}$$

where $p_\phi := \prod_{1\leq k\leq l} p_{f(k)}$ denotes the probability of the fault-sequence $\phi \in F^l$, in which the notation $f(k) \in F$ denotes the kth fault in the fault-sequence $\phi \in F^l$.

Unlike TSM, CCT, RM, and LSM, the resilience measures LL and RT are inversely correlated with the level of resilience (i.e., a higher resilience corresponds to a lower LL or a lower RT). Hence, to define the overall resilience measure in (30), the "complements" $(1 - nLL_\phi)$ and $(1 - nRT_\phi)$ of the normalized LL and RT values are used, measuring the normalized levels of load served and system uptime, respectively. To a

system designer or evaluator, such six-dimensional measure $R_l \in [0,1]^6$ forms a basis to compare the resilience of different designs. To compare/evaluate a number of designs, a designer may require certain minimum acceptable levels for each of the 6 indices, and among the designs that are acceptable, they may rank highest the one with the largest $||R_l||_1$ or $||R_l||_2$ value, or top-most value per a lexicographical ordering based on their relative preference of the 6 measures.

A. Deriving Time Integral of Load Served

Here, we show that a recently reported measure of resilience, namely, TILS over a finite time-window [9], can be derived from our proposed set of 6 measures. For a fault-recovery timed-sequence $\psi = ((a_1, t_1), \ldots, (a_l, t_l)) \in \Psi$, its TILS can be derived as

$$\text{TILS}_\psi = t_l \cdot L_0 - \sum_{i=1}^{l-1} \left(\sum_{r \in I_{\phi(i)}} \text{LL}_{\phi(i),r} \right) \times (t_{i+1} - t_i) \quad (31)$$

where L_0 is the load connected to the initial system, and $\phi(i)$ denotes the sequence of *active* faults in ψ at time t_i (i.e., faults that are yet to recover by time t_i). The overall TILS against the set of all length-l fault-sequences in F^l is then given by the probabilistic average

$$\text{TILS}_l = \sum_{\psi \in \Psi} p_\psi \text{TILS}_\psi. \quad (32)$$

The TILS of (31) is similar to that proposed as a resilience metric in [9] and used in [10]. Our proposed set of indices in (30) provides a more comprehensive measure of resilience.

V. Implementation and Test System Results

The overall framework of computing the composite resilience indices is implemented in MATLAB, where we used: SPOT [46] for inner approximation of the RoS, CVX [47] to compute the volume of the approximate RoS and the RM, PSAT [48] with necessary extension to compute the LSM and the LL and a self-developed module for solving the power-flow and the time domain simulation. MOSEK [49], a commercial optimization tool, was used as the backend optimizer for both SPOT and CVX.

A. Resilience Comparison for 3 Illustrative Power Systems

In order to demonstrate the effectiveness of the proposed approach, we apply it on three similar 3-machine-7-bus systems, and compute and compare their resilience levels against all fault-sequences of length 2. All three systems have the same set of generators, loads, transformers, and lines; they only differ in the location of the generators. Yet it turns out that the three systems have different levels of resilience over the set of all possible fault-sequences. The three systems, referred as PS_1, PS_2, and PS_3, are shown in Fig. 4(a)–(c), respectively. The corresponding system data can be found in Appendix C of the extended version of this article [42].

For comparing the resilience levels of the three chosen systems PS_1, PS_2, and PS_3, we assumed that their RTs are identical (since their system topologies and components are the same), and hence, the RT is not a factor in computing their overall composite resilience measures. Among the considered faults: 1) line fault; 2) transformer fault; 3) bus fault; and 4) generator outage, the first three are modeled by the application of symmetric three phase fault at one of the system components of the respective type. The total number of the faults of interest for each system equals the total number of components, namely, 18. The sequencing of two of these faults leads to a total of 194 length-2 "feasible" fault-sequences that we analysed for each of the three systems. First, the set of all live subsystems $\mathcal{I}_L$ is obtained by applying and clearing all length-2 fault-sequences and their prefixes. PS_1 was found to have a total of 224 possible live subsystems, while that number for each of PS_2 and PS_3 was found to be 216.

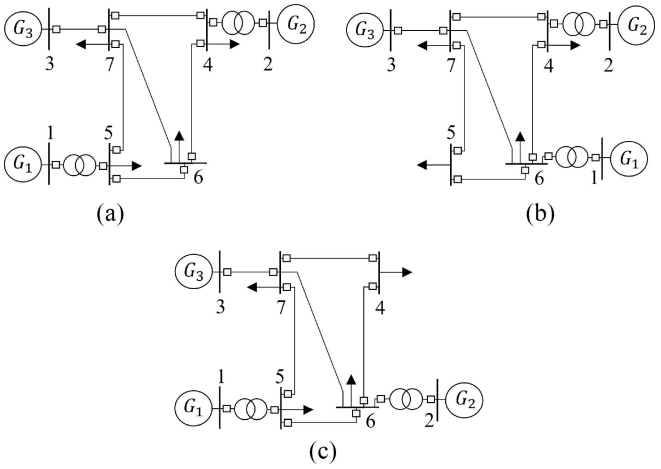

Fig. 4. Single line diagrams of illustrative 7-bus systems. (a) PS_1. (b) PS_2. (c) PS_3.

The fault-clearance time was chosen to be 60 ms [27] (i.e., approximately 4 cycles for a 60 Hz system). A bus fault was cleared by isolating the bus from the system, disconnecting all the lines, generators, and transformers connected to the faulty bus. A line or a transformer fault was cleared by opening the adjacent breakers and thus, removing the faulty component. The other computation parameters were set as: $p = [0.75, 0.1, 0.05, 0.1]^T$ and $\alpha = 1$. Here, p is a 4-D fault probability vector (element-wise for line, transformer, bus, and generator faults, respectively).

Fig. 5(a)–(e) shows the computed normalized values of the respective resilience measures TSM, CCT, RM, LSM, and LL for the three systems in 1-D vertical scatter plots (each scatter plot has 194 circles indicating the values corresponding to the 194 length-2 fault-sequences, respectively). The stars on the scatter plots correspond to the probabilistically averaged values of the resilience measures of the respective systems.

Table I lists the averaged resilience measures R_2 for the three systems, along with their 1- and 2-norms: $||R_2||_1$ and $||R_2||_2$. The complete set of results tabulating all the $194 \times 3 = 582$ length-2 fault-sequences is presented in Appendixes D–F of the extended version of this article [42]. PS_2 evaluates to be the least resilient system topology among the three since it is the lowest in majority of the five indices of R_2. Based on the $||R_2||_1$ or $||R_2||_2$ values, PS_3 is found to be the most

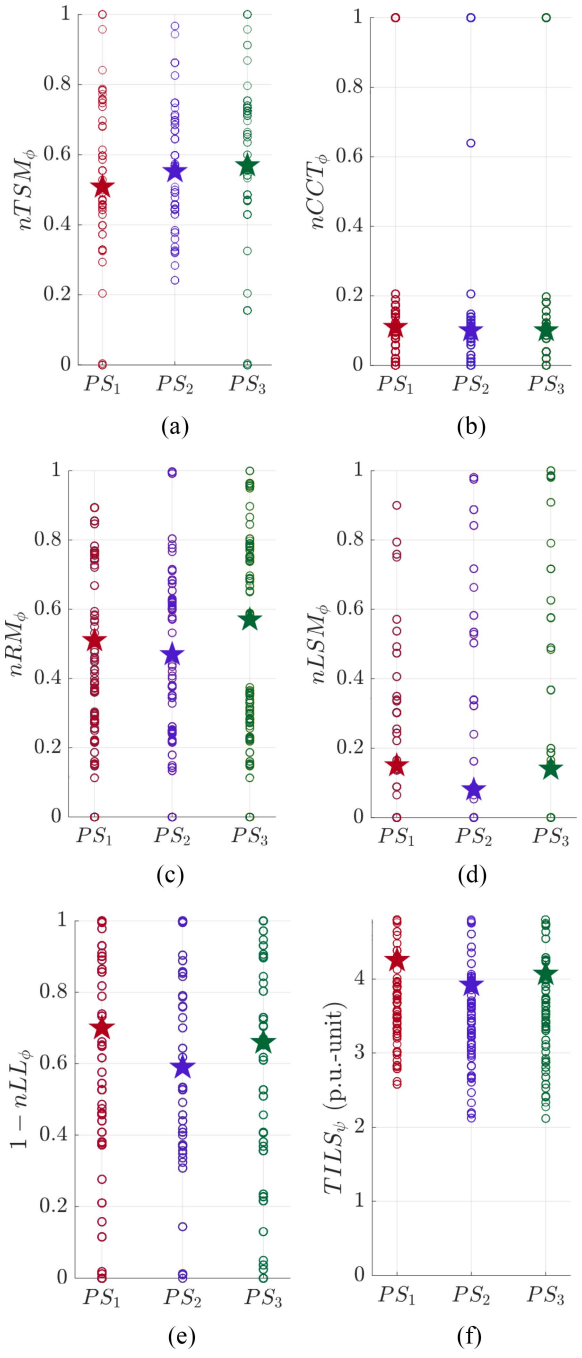

Fig. 5. 1-D scatter plots of the normalized resilience measures. (a) TSM. (b) CCT. (c) RM. (d) LSM. (e) LL and the "unnormalized" index. (f) TILS_ψ for the three systems PS_1, PS_2, and PS_3 against all length-2 fault-sequences. The stars correspond to the probabilistically weighted-averaged values of the resilience measures.

resilient among the three. This ranking is appropriate when all the five measures are equally important to the operator. On the other hand, if the amount of load served is of higher priority as compared to the stability or RM, then the operator may choose PS_1 over PS_3 based on the computed R_2.

For computing TILS for our test example of three systems, we treat the interval $t_{i+1} - t_i \ \forall i \in \{1, \ldots, l-1\}$ to be constant, say τ, which implies a constant RT for each fault, consistent with the earlier assumption in this section. For

TABLE I
COMPARISON OF RESILIENCE MEASURES

System	$\lvert F^2\rvert$	$\lvert\mathcal{I}_L\rvert$	R_2	$\lvert\lvert R_2\rvert\rvert_1$	$\lvert\lvert R_2\rvert\rvert_2$
PS_1	194	224	[0.51 0.11 0.51 0.15 0.70]	1.97	1.02
PS_2	194	216	[0.55 0.10 0.49 0.08 0.59]	1.82	0.95
PS_3	194	216	[0.57 0.10 0.57 0.13 0.66]	2.03	1.05

$t_l = 1.5$ unit, $\tau = 0.5$ unit, and L_0 and $\text{LL}_{\phi(i),r}$ measured in p.u., Fig. 5(f) shows the computed values of TILS_ψ for the three systems PS_1, PS_2, and PS_3 in a vertical scatter plot, where their corresponding probabilistically averaged values TILS_2, marked as stars, are 4.25, 3.92, and 4.07, respectively. With respect to their TILS measures, the systems can be ranked as: $\text{PS}_1 > \text{PS}_3 > \text{PS}_2$. This order is different from the one obtained using an aggregate of all 6 proposed measures as captured in the norms $||R_2||_1$ or $||R_2||_2$, namely, $\text{PS}_3 > \text{PS}_1 > \text{PS}_2$. In other words, using only the TILS-based resilience measure that depends only on the LL and RT, can in general be limiting, when compared to the proposed full set of 6 indices.

B. Implementation on IEEE 30-Bus Test System

To further validate the applicability of our proposed framework, we implemented it on the IEEE 30-bus test system [50] that is widely employed in various applications; some recent examples include: [51]–[55]. It models a portion of the American Electric Power System in the midwestern U.S, which includes 6 synchronous generators, 4 transformers, 29 buses, and 34 lines, and can witness a total of 73 different faults. Fig. 6 shows the single-line diagram of the model. Note in the single-line diagram, the three transformers 6-9, 9-10, and 9-11 together represent a single 3-winding transformer, and similarly, the transformers 4-12 and 12-13 together represent another 3-winding transformer (see [50] for more details).

The system's security limits pertaining to line-currents and bus-voltages were obtained from [56]. Table II shows the parameters related to the six generators, such as their MVA ratings, base-case dispatch schedule, reactive power upper/lower limits (taken from [56]), transient direct-axis reactance (i.e., the imaginary part of z_i in (2), denoted by $x_{d,i}$ hereinafter) and the parameters M_i and D_i of the classical dynamic model. Table II shows the per unit (p.u.) values for the respective generators converted to a common system base of 100 MVA. The machine-base values of $x_{d,i} = 0.25$ p.u., $M_i = 8.68$ s. (both taken from the default values of round-rotor generator model available in PSS/E [57]), and $D_i = 3$ (taken from [58]) are identical for all six generators.

By virtue of the six generators (i.e., $N = 6$) present in the model, the model of (6) has 11 state variables, and upon the polynomialization as in (8), it contains 16 state variables. The estimated RoS of the base-case system (prior to occurrence of any faults) using the proposed SoS-based method, projected on to the 2-D spaces of every pairs of the relative angles, is shown in Fig. 7. The steady state variation of a few

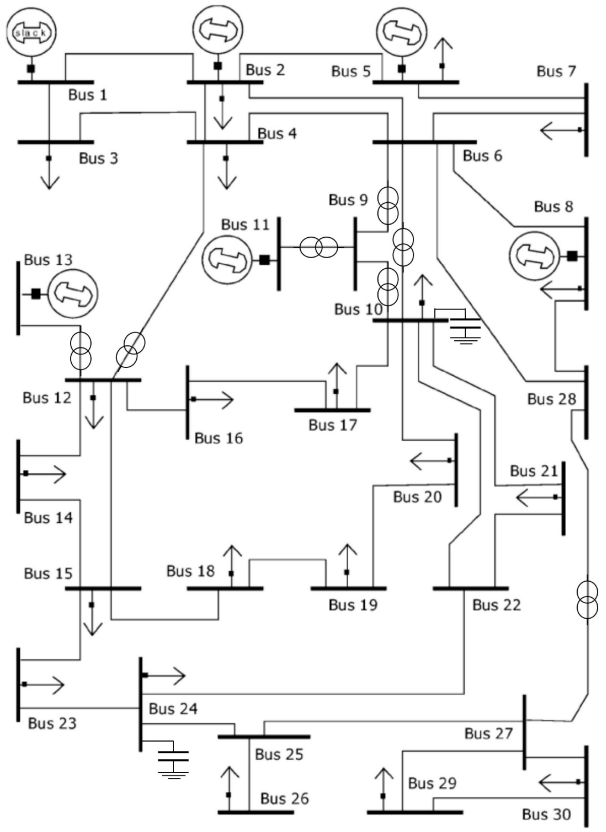

Fig. 6. Single-line diagram of the IEEE 30-bus test system.

TABLE II
GENERATOR DATA USED IN IEEE 30-BUS SYSTEM

Generator (Bus #)	Rated MVA	P_G (p.u.)	$Q_{G,max}$ (p.u.)	$Q_{G,min}$ (p.u.)	$x_{d,i}$ (p.u.)	M_i (sec.)	D_i
1	250	0.21	0.88	-0.2	0.1	21.7	7.5
2	100	0.68	0.35	-0.2	0.25	8.68	3
5	80	0.55	0.28	-0.15	0.3125	6.944	2.4
8	60	0.55	0.21	-0.15	0.4167	5.208	1.8
11	50	0.40	0.25	-0.1	0.5	4.34	1.5
13	60	0.47	0.35	-0.15	0.4167	5.208	1.8

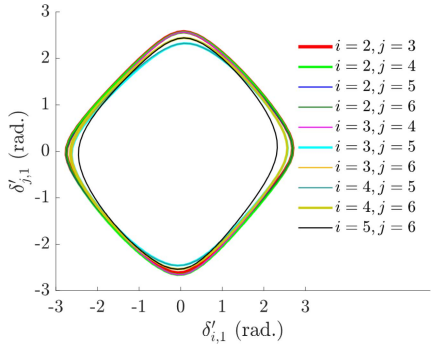

Fig. 7. Estimated RoS of IEEE 30-bus test system with the origin set as the equilibrium, projected on the 2-D space of all pairs of relative generator angles.

representative load-bus voltages with increase in the loads and the generations from their nominal values is shown in Fig. 8.

Following the method proposed in Sections III–IV, we compute the resilience measures TSM, CCT, RM, LSM,

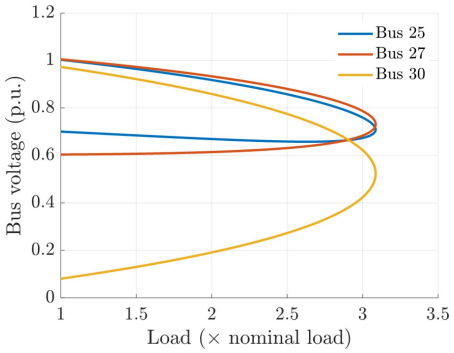

Fig. 8. Steady state variation of voltages at representative load-buses 25, 27, and 30 of IEEE 30-bus test system, with increase in load from nominal value.

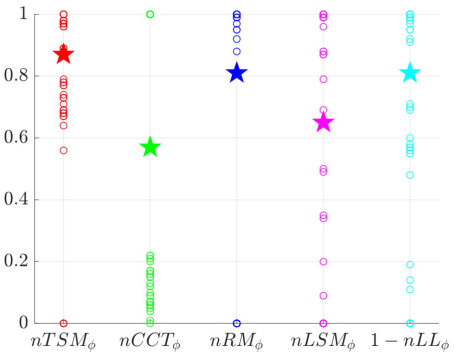

Fig. 9. 1-D scatter plots of the normalized resilience measures: TSM, CCT, RM, LSM, and LL for the IEEE 30-bus system against all 73 length-1 faults. The stars correspond to the probabilistically weighted-averaged values.

and LL and their normalized values for all 73 faults. The fault properties and resilience computation related parameters are considered same as those used for the illustrative 7-bus systems. To allow for reconfiguration/resourcefulness, prior to computing LSM and LL for each fault scenario, we allowed adjustment of generation schedule and/or switching of the shunt capacitors at buses 10 and 24. The 1-D vertical scatter plots in Fig. 9 show the computed normalized values of the respective resilience measures TSM, CCT, RM, LSM, and LL (in red, green, blue, magenta, and cyan colors, respectively), where the circles indicate their values under different faults, and the stars indicate the corresponding probabilistic averages. A detailed table including the values of the resilience indices is provided in Appendix G of the extended version [42].

C. Comments on Computational Complexity and Scalability

The most computationally complex part of our proposed method is the inner approximation of the RoS, which involves solving the SoS feasibility problems. This being polynomial in the number of generators in the system, has also become scalable. On our 64 bit computer with 16 GB RAM and 2.6 GHz processor, the computation of the proposed resilience indices for each fault-sequence took about 10 s on average for the illustrative systems, while that time for the IEEE 30-bus system was 25 min. The typical industry practice of time-domain simulation is itself limited to a single

sequence of faults, and it must be repeated while simulating other fault-sequences. Our approach, being polynomial per fault-sequence, remains comparable, yet it quantifies the resilience levels that a time-domain simulation by itself cannot do. It also helps to note that in evaluating alternative designs for N-1 or N-2 or N-3 levels of resilience, only a polynomial number of fault-sequences is required to be analyzed (i.e., of the order of #faults^3), making the computation practical. Also, since such computations for each fault-sequence and the resulting subsystem(s) can be executed in parallel, the proposed composite resilience metric can be parallelized, making it computationally scalable and attractive.

VI. Conclusion

A resilience measure of a dynamical cyberphysical system (CPS), such as a power system, must capture its ability to offer performance stably against the ensuing faults/attacks. Accordingly, we proposed a novel composite resilience measure that quantifies stability-level against faults in forms of TSM, CCT, RM, and LSM, and the performance-level in forms of LL and RT. To the best of our knowledge, this is the first such comprehensive quantification of resilience for a power system, one that also applies to any dynamical CPS (by replacing RM and LSM with appropriate safety margins, and LL with suitable quality-of-service loss). The 6 proposed measures are computed for each prefix of a fault-sequence and for each resulting subsystem, and are aggregated (through minimization or summation) to find the respective measures for the fault-sequence. After being computed for all individual fault-sequences, these measures are normalized and finally averaged against the occurrence probabilities of the fault-sequences to obtain the overall resilience measure, a composite of 6 unit-interval resilience indices. These indices provide a useful basis to decide the need of strengthening the system's configurations to enhance its level of resilience. The proposed set of measures are much more comprehensive compared to other existing ones, e.g., the resilience metric of TILS, which can be derived using just two of the six proposed measures, namely, LL and RT.

For computing the size of the RoS, we proposed a novel approach that builds on the existing SoS optimization based technique yielding a polynomial complexity computation (in the number of generators), and further used it to also estimate the CCT. We also proposed a new quadratic optimization approach to compute the RM. Finally, we introduced the security and stability constrained notions of LSM and LL and implemented the CPF method for their computation. The proposed computation scheme is of polynomial complexity in the number of generators, and is further amenable to parallel computing, making it scalable. For the first time, the SoS optimization-based RoS estimation was conducted for a practical test system, so as to analyze transient stability as well as CCT under various fault-sequences and post-clearance reconfigurations.

The proposed composite resilience measure is helpful in expressing the relative resilience of different power systems, under sequence of faults. This can be a useful tool in the planning phase, for example, to select the most desirable system topology among multiple viable ones. Also, for any fault-sequence, a smaller resilience measure would signify a higher severity, and thus, the approach also provides a basis for screening the fault-sequences for further detailed analysis according to their severity in terms of both loss of stability and performance levels.

Acknowledgment

The authors thank Prof. M. A. Pai, University of Illinois Urbana Champaign, for his useful comments during the course of this research.

References

[1] *DHS Risk Lexicon 2010 Edition*, DHS Risk Steering Committee, London, U.K., 2010.

[2] I. Dobson, B. A. Carreras, D. E. Newman, and J. M. Reynolds-Barredo, "Obtaining statistics of cascading line outages spreading in an electric transmission network from standard utility data," *IEEE Trans. Power Syst.*, vol. 31, no. 6, pp. 4831–4841, Nov. 2016.

[3] "Definition and classification of power system stability," in *Electra*, i-Force, Erpe-Mere, Belgium, 2003, pp. 74–80.

[4] *Transmission System Planning Performance Requirements*. Accessed: May 1, 2020. [Online]. Available: https://www.nerc.com/_layouts/15/PrintStandard.aspx?standardnumber=TPL-001-4&title=Transmission%20System%20Planning%20Performance%20Requirements&jurisdiction=United%20States

[5] A. Berkeley, M. Wallace, and C. Coo, "A framework for establishing critical infrastructure resilience goals," in *Final Report and Recommendations by the Council*, Nat. Infrastruct. Advisory Council, Washington, DC, USA, 2010.

[6] M. Ibrahim, J. Chen, and R. Kumar, "A resiliency measure for electrical power systems," in *Proc. IEEE 13th Int. Workshop Discrete Event Syst. (WODES)*, Xi'an, China, 2016, pp. 385–390.

[7] L. Jin, R. Kumar, and N. Elia, "Reachability analysis based transient stability design in power systems," *Int. J. Elect. Power Energy Syst.*, vol. 32, no. 7, pp. 782–787, 2010.

[8] N. A. Samaan, J. Dagle, Y. Makarov, R. Diao, and M. Vallem, "Dynamic contingency analysis tool–phase 1," Pac. Northwest Nat. Lab., Richland, WA, USA, Rep. 24843, 2015.

[9] M. Panteli, P. Mancarella, D. N. Trakas, E. Kyriakides, and N. D. Hatziargyriou, "Metrics and quantification of operational and infrastructure resilience in power systems," *IEEE Trans. Power Syst.*, vol. 32, no. 6, pp. 4732–4742, Nov. 2017.

[10] S. Zuloaga, P. Khatavkar, L. Mays, and V. Vittal, "Resilience of cyber-enabled electrical energy and water distribution systems considering infrastructural robustness under conditions of limited water and/or energy availability," *IEEE Trans. Eng. Manag.*, early access, Sep. 18, 2019, doi: 10.1109/TEM.2019.2937728.

[11] P. A. Parrilo, "Structured semidefinite programs and semialgebraic geometry methods in robustness and optimization," Ph.D. dissertation, Dept. Doctor Philos., California Inst. Technol., Pasadena, CA, USA, 2000.

[12] Y. Zhu, D. Zhao, X. Yang, and Q. Zhang, "Policy iteration for h_∞ optimal control of polynomial nonlinear systems via sum of squares programming," *IEEE Trans. Cybern.*, vol. 48, no. 2, pp. 500–509, Feb. 2018.

[13] S. Izumi, H. Somekawa, X. Xin, and T. Yamasaki, "Estimation of regions of attraction of power systems by using sum of squares programming," *Elect. Eng.*, vol. 100, no. 4, pp. 2205–2216, 2018.

[14] M. Anghel, F. Milano, and A. Papachristodoulou, "Algorithmic construction of Lyapunov functions for power system stability analysis," *IEEE Trans. Circuits Syst. I, Reg. Papers*, vol. 60, no. 9, pp. 2533–2546, Sep. 2013.

[15] S. Boyd and L. Vandenberghe, *Convex Optimization*. Cambridge, U.K.: Cambridge Univ. Press, 2004.

[16] M. Pai, *Energy Function Analysis for Power System Stability*. Boston, MA, USA: Springer, 2012.

[17] H.-D. Chiang, *Direct Methods for Stability Analysis of Electric Power Systems: Theoretical Foundation, BCU Methodologies, and Applications*. Hoboken, NJ, USA: Wiley, 2011.
[18] C.-C. Chu and H.-D. Chiang, "Boundary properties of the BCU method for power system transient stability assessment," in *Proc. IEEE Int. Symp. Circuits Syst.*, Paris, France, 2010, pp. 3453–3456.
[19] M. Pai and P. W. Sauer, "Stability analysis of power systems by Lyapunov's direct method," *IEEE Control Syst. Mag.*, vol. 9, no. 1, pp. 23–27, Jan. 1989.
[20] N. Kakimoto, Y. Ohsawa, and M. Hayashi, "Transient stability analysis of multimachine power system with field flux decays via Lyapunov's direct method," *IEEE Trans. Power App. Syst.*, vol. PAS-99, no. 5, pp. 1819–1827, Sep. 1980.
[21] J. L. Willems and J. C. Willems, "The application of Lyapunov methods to the computation of transient stability regions for multimachine power systems," *IEEE Trans. Power App. Syst.*, vol. PAS-89, no. 5, pp. 795–801, May 1970.
[22] D. J. Hill and C. N. Chong, "Lyapunov functions of lur'e-postnikov form for structure preserving models of power systems," *Automatica*, vol. 25, no. 3, pp. 453–460, 1989.
[23] R. Ortega, M. Galaz, A. Astolfi, Y. Sun, and T. Shen, "Transient stabilization of multimachine power systems with nontrivial transfer conductances," *IEEE Trans. Autom. Control*, vol. 50, no. 1, pp. 60–75, Jan. 2005.
[24] H.-D. Chang, C.-C. Chu, and G. Cauley, "Direct stability analysis of electric power systems using energy functions: Theory, applications, and perspective," *Proc. IEEE*, vol. 83, no. 11, pp. 1497–1529, Nov. 1995.
[25] F. Dobraca, M. Pai, and P. Sauer, "Relay margins as a tool for dynamical security analysis," *Int. J. Elect. Power Energy Syst.*, vol. 12, no. 4, pp. 226–234, 1990.
[26] H. Bai and V. Ajjarapu, "Relay margin trajectory based identification of transmission vulnerability for power system security assessment," in *Proc. IEEE iREP Symp. Bulk Power Syst. Dyn. Control VII Revitalizing Oper. Rel.*, Charleston, SC, USA, 2007, pp. 1–9.
[27] S. Soman, T. B. Nguyen, M. Pai, and R. Vaidyanathan, "Analysis of angle stability problems: A transmission protection systems perspective," *IEEE Trans. Power Del.*, vol. 19, no. 3, pp. 1024–1033, Jul. 2004.
[28] V. Ajjarapu and C. Christy, "The continuation power flow: A tool for steady state voltage stability analysis," in *Proc. IEEE Conf. Papers Power Ind. Comput. Appl. Conf.*, Baltimore, MD, USA, 1991, pp. 304–311.
[29] R. Kinney, P. Crucitti, R. Albert, and V. Latora, "Modeling cascading failures in the north American power grid," *Eur. Phys. J. B, Condens. Matter Complex Syst.*, vol. 46, no. 1, pp. 101–107, 2005.
[30] P. J. Maliszewski and C. Perrings, "Factors in the resilience of electrical power distribution infrastructures," *Appl. Geogr.*, vol. 32, no. 2, pp. 668–679, 2012.
[31] R. Francis and B. Bekera, "A metric and frameworks for resilience analysis of engineered and infrastructure systems," *Rel. Eng. Syst. Safety*, vol. 121, pp. 90–103, Jan. 2014.
[32] M. Ouyang and L. Dueñas-Osorio, "Resilience modeling and simulation of smart grids," in *Proc. Struct. Congr.*, 2011, pp. 1996–2009.
[33] P. E. Roege, Z. A. Collier, J. Mancillas, J. A. McDonagh, and I. Linkov, "Metrics for energy resilience," *Energy Policy*, vol. 72, pp. 249–256, Sep. 2014.
[34] H. H. Willis and K. Loa, *Measuring The Resilience of Energy Distribution Systems*. Santa Monica, CA, USA: RAND Corp., 2015.
[35] R. Arghandeh, A. Von Meier, L. Mehrmanesh, and L. Mili, "On the definition of cyber-physical resilience in power systems," *Renew. Sustain. Energy Rev.*, vol. 58, pp. 1060–1069, May 2016.
[36] R. Filippini and A. Silva, "I (R)ML: An infrastructure resilience-oriented modeling language," *IEEE Trans. Syst., Man, Cybern., Syst.*, vol. 45, no. 1, pp. 157–169, Jan. 2015.
[37] H. Fujita, A. Gaeta, V. Loia, and F. Orciuoli, "Resilience analysis of critical infrastructures: A cognitive approach based on granular computing," *IEEE Trans. Cybern.*, vol. 49, no. 5, pp. 1835–1848, May 2019.
[38] X. Zeng, Z. Liu, and Q. Hui, "Energy equipartition stabilization and cascading resilience optimization for geospatially distributed cyber-physical network systems," *IEEE Trans. Syst., Man, Cybern., Syst.*, vol. 45, no. 1, pp. 25–43, Jan. 2015.
[39] H. K. Khalil, *Nonlinear Control*. New York, NY, USA: Pearson, 2015.
[40] S. Talukder and R. Kumar, "An enhancement in sum-of-squares optimization based region of attraction estimation for power systems," in *Proc. IEEE Power Energy Soc. Gen. Meeting (PESGM)*, Atlanta, GA, USA, 2019, pp. 1–5.
[41] J. Bochnak, M. Coste, and M.-F. Roy, *Real Algebraic Geometry*, vol. 36. Berlin, Germany: Springer-Verlag, 1998.
[42] S. Talukder, M. Ibrahim, and R. Kumar. (2020). *Resilience Indices for Power/Cyberphysical Systems: Extended Version*. [Online]. Available: https://drive.google.com/file/d/1DfDB3XDMEA1QP6TB9Ml2_EikfCrXudLG/view?usp=sharing
[43] M.-Y. Chow, L. S. Taylor, and M.-S. Chow, "Time of outage restoration analysis in distribution systems," *IEEE Trans. Power Del.*, vol. 11, no. 3, pp. 1652–1658, Jul. 1996.
[44] J. R. A. Rodriguez and A. Vargas, "Fuzzy-heuristic methodology to estimate the load restoration time in MV networks," *IEEE Trans. Power Syst.*, vol. 20, no. 2, pp. 1095–1102, May 2005.
[45] A. Jaech, B. Zhang, M. Ostendorf, and D. S. Kirschen, "Real-time prediction of the duration of distribution system outages," *IEEE Trans. Power Syst.*, vol. 34, no. 1, pp. 773–781, Jan. 2019.
[46] A. A. Ahmadi and A. Majumdar, "DSOS and SDSOS optimization: More tractable alternatives to sum of squares and semidefinite optimization," *SIAM J. Appl. Algebra Geom.*, vol. 3, no. 2, pp. 193–230, 2019.
[47] M. Grant and S. Boyd. (Sep. 2013). *CVX: MATLAB Software for Disciplined Convex Programming, Version 2.0 Beta*. [Online]. Available: http://cvxr.com/cvx
[48] F. Milano, "An open source power system analysis toolbox," *IEEE Trans. Power syst.*, vol. 20, no. 3, pp. 1199–1206, Aug. 2005.
[49] E. D. Andersen and K. D. Andersen, "The mosek interior point optimizer for linear programming: An implementation of the homogeneous algorithm," in *High Performance Optimization*. Boston, MA, USA: Springer, 2000, pp. 197–232.
[50] *Power Systems Test Case Archive*, Univ. Washington, Seattle, WA, USA, 1961. [Online]. Available: http://labs.ece.uw.edu/pstca/pf30/pg_tca30bus.htm
[51] S. S. Torbaghan *et al.*, "Optimal flexibility dispatch problem using second-order cone relaxation of AC power flows," *IEEE Trans. Power Syst.*, vol. 35, no. 1, pp. 98–108, Jan. 2020.
[52] S. A. Saleh, J. Wo, X. F. St-Onge, and E. Castillo-Guerra, "A new approach for estimating frequency variations due to smart grid functions," *IEEE Trans. Ind. Appl.*, vol. 56, no. 3, pp. 2292–2303, May/Jun. 2020.
[53] A. Nikoobakht, J. Aghaei, H. R. Massrur, and R. Hemmati, "Decentralised hybrid robust/stochastic expansion planning in coordinated transmission and active distribution networks for hosting large-scale wind energy," *IET Gener. Transm. Distrib.*, vol. 14, no. 5, pp. 797–807, Mar. 2020.
[54] S. S. Reddy and J. A. Momoh, "Realistic and transparent optimum scheduling strategy for hybrid power system," *IEEE Trans. Smart Grid*, vol. 6, no. 6, pp. 3114–3125, Nov. 2015.
[55] M. Althoff, "Formal and compositional analysis of power systems using reachable sets," *IEEE Trans. Power Syst.*, vol. 29, no. 5, pp. 2270–2280, Sep. 2014.
[56] O. Alsac and B. Stott, "Optimal load flow with steady-state security," *IEEE Trans. Power App. Syst.*, vol. PAS-93, no. 3, pp. 745–751, May 1974.
[57] *PSS/E Model Library of PSS/E-32*, PSSőE Siemens, Schenectady, NY, USA, 2009.
[58] V. Vittal, J. D. McCalley, P. M. Anderson, and A. Fouad, *Power System Control and Stability*. Chichester, U.K.: Wiley, 2019.

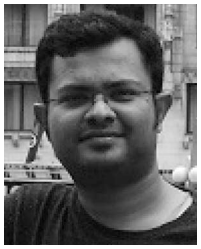

Soumyabrata Talukder (Graduate Student Member, IEEE) received the bachelor's degree in electrical engineering from Jadavpur University, Kolkata, India, in 2009. He is currently pursuing the Ph.D. degree in electrical engineering with the Department of Electrical and Computer Engineering, Iowa State University, Ames, IA, USA.

He served as a Project Engineer with GE Grid Solutions (formerly, Alstom Grid), India, from 2009 to 2012, and thereafter, as an Assistant Manager with Central Projects Organization, ITC Ltd., Kolkata, India, from 2012 to 2017. His current research interests include resilience of complex systems, polynomial optimization, machine learning, stability guaranteed reinforcement learning, and coalition games with power systems as the application domain.

Mariam Ibrahim (Member, IEEE) received the bachelor's degree in electrical and computer engineering from Hashemite University, Zarqa, Jordan, in 2008, the M.S. degree in mechatronics engineering from Al Balqa Applied University, Salt, Jordan, in 2011, and the Ph.D. degree in electrical engineering from Iowa State University, Ames, IA, USA, in 2016.

She is an Assistant Professor with German Jordanian University, Amman, Jordan, which also sponsored her Ph.D. studies. Her research interests include cyber physical systems security and resiliency analysis, and artificial learning-based algorithms.

Ratnesh Kumar (Fellow, IEEE) received the B.Tech. degree in electrical engineering from the Indian Institute of Technology Kanpur, Kanpur, India, in 1987, and the M.S. and Ph.D. degrees in electrical and computer engineering from the University of Texas at Austin, Austin, TX, USA, in 1989 and 1991, respectively.

He is a Harpole Professor with the Department of Electrical and Computer Engineering, Iowa State University, Ames, IA, USA, where he directs the ESSeNCE ("Embedded Software, Sensors, Networks, Cyberphysical, an Energy") Laboratory. He held faculty position with the University of Kentucky, Lexington, Kentucky, and also visiting positions with the University of Maryland, College Park, MD, USA, the Applied Research Laboratory, Pennsylvania State University, State College, PA, USA, NASA Ames, Mountain View, CA, USA, Idaho National Laboratory, Idaho Falls, ID, USA, United Technologies Research Center, East Hartford, CT, USA, General Electric Global Research, Niskayuna, NY, USA, and Wright Patterson Air Force Research Laboratory, Wright-Patterson AFB, OH, USA.

Dr. Kumar received the D. R. Boylan Eminent Faculty Award for Research at Iowa State University, the Gold Medals for the Best EE Undergrad, the Best EE Project, the Best All Rounder from IIT Kanpur in 1987, the Best Dissertation Award from UT Austin in 1991, the Best Paper Award from the IEEE TRANSACTIONS ON AUTOMATION SCIENCE AND ENGINEERING in 2016, and the Keynote Speakership and best paper awards recipient from multiple conferences. He was a Distinguished Lecturer of IEEE Control Systems Society. He is or has been an editor for several journals (including of IEEE, SIAM, ACM, IET, and MDPI). He is also a Fellow of AAAS.